Mon. Not. R. Astron. Soc. **000**, 1–13 (2016) Printed August 30, 2016 (MN LATEX style file v2.2)

Radial Variation in the Stellar Mass Functions of Star Clusters

Jeremy J. Webb & Enrico Vesperini ⋆
Department of Astronomy, Indiana University, Swain West, 727 E. 3rd Street, IN 47405 Bloomington, USA

August 30, 2016

arXiv:1608.07293v2 [astro-ph.GA] 29 Aug 2016

ABSTRACT

A number of recent observational studies of Galactic globular clusters have measured the variation in the slope of a cluster's stellar mass function α with clustercentric distance r. In order to gather a deeper understanding of the information contained in such observations, we have explored the evolution of $\alpha(r)$ for star clusters with a variety of initial conditions using a large suite of N-body simulations. We have specifically studied how the time evolution of $\alpha(r)$ is affected by initial size, mass, binary fraction, primordial mass segregation, black hole retention, an external tidal field, and the initial mass function itself. Previous studies have shown that the evolution of α_G is closely related to the amount of mass loss suffered by a cluster. Hence for each simulation we have also followed the evolution of the slope of the cluster's global stellar mass function, α_G, and have shown that clusters follow a well-defined track in the α_G-$d\alpha(r)/d(ln(r/r_m))$ plane. The location of a cluster on the $\alpha_G - d\alpha(r)/d(ln(r/r_m))$ plane can therefore constrain its dynamical history and, in particular, constrain possible variations in the stellar initial mass function. The α_G-$d\alpha(r)/d(ln(r/r_m))$ plane thus serves as a key tool for fully exploiting the information contained in wide field studies of cluster stellar mass functions.

Key words: galaxies: star clusters (Galaxy:)globular clusters: general stars: kinematics and dynamics stars:statistics

1 INTRODUCTION

The two mechanisms which dominate the dynamical evolution of any globular cluster are stellar evolution and two-body relaxation. For globular clusters which survive their formation environment (e.g. Gieles et al. 2006; Kruijssen et al. 2011, 2012; Renaud & Gieles 2013; Rieder et al. 2013), stellar evolution is the initial driver behind cluster evolution and early expansion due to mass loss from high-mass stars. After this early stage, two-body relaxation takes over and the cluster evolves towards a state of partial energy equipartition (Merritt 1981; Miocchi 2006; Trenti & van der Marel 2013; Gieles & Zocchi 2015; Bianchini et al. 2016). A natural result of two-body relaxation is the segregation of higher mass stars towards the cluster center while lower mass stars migrate outwards (e.g. Heggie & Hut 2003). Two-body relaxation will also eventually lead to cluster dissolution as stars are energized to velocities greater than the cluster's escape velocity and pushed beyond the tidal radius r_t imposed by the tidal field of the host galaxy. In the presence of a non-static external tidal field, tidal heating and shocks serve to inject energy and further accelerate the dissolution process (e.g. Weinberg 1994; Vesperini & Heggie 1997; Gnedin et al. 1999; Baumgardt & Makino 2003; Webb et al. 2013, 2014a,b; Brockamp et al. 2014).

At early times, evolution of the stellar mass function is only affected by stellar evolution as massive stars lose mass. The early loss of outer stars associated with the expansion triggered by stellar evolution mass loss will not affect the mass function unless the cluster is primordially mass segregated (e.g. Baumgardt, De Marchi & Kroupa 2008; Vesperini et al. 2009; Haghi et al. 2015). However as a cluster undergoes mass segregation, the mean mass of escaping stars will decrease over time which will cause the slope of the mass function to flatten (become less negative). The combined effects of stellar evolution, two-body relaxation, and the presence of an external tidal field on the stellar mass function have been well studied throughout the literature (e.g. Vesperini & Heggie 1997; Kruijssen 2009; Baumgardt & Makino 2003; Trenti et al. 2010; Leigh et al. 2012; Lamers et al. 2013; Webb et al. 2014a; Webb & Leigh 2015). These studies have shown that the *global* stellar mass function is primarily a function of the fraction of mass lost

⋆ E-mail: jerjwebb@iu.edu (JW), evesperi@indiana.edu (EV)

by a cluster, with some scatter about the relation due to the amount of mass segregation a cluster undergoes before it starts to lose a significant amount of stars. Additional factors that have been shown to at least partially influence the evolution of the stellar mass function as a function of fraction of mass lost include the total dissolution time of the cluster (Kruijssen 2009), the initial binary fraction and initial mass function (IMF) (Webb & Leigh 2015), the retention fraction of dark remnants (Trenti et al. 2010; Lutzgendorf et al. 2013), and the presence of an intermediate mass black hole (Lutzgendorf et al. 2013).

In Webb et al. (2014a), the effects of an external tidal field on the evolution of the stellar mass function *at different clustercentric radii* was explored for clusters with circular and eccentric orbits. The slope of the mass function expectedly increases in the inner regions and decreases in the outer regions as stars within the cluster segregate. Webb et al. (2014a) also found that an external field will influence the mass function beyond the half-mass radius r_m by preferentially stripping stars in the outer regions which, as a result of the cluster's evolution towards partial energy equipartition, are dominated by low-mass stars.

With continuing advancements in telescope capabilities and observational techniques, it has become possible to reliably measure the mass function of Galactic globular clusters at different clustercentric radii. Such measurements allow for a study of the radial variation of the mass function, and have been done recently for M10 (Beccari et al. 2010), Pal 4 (Frank et al. 2012), Pal 14 (Frank et al. 2014), NGC 6101 (Dalessandro et al. 2015), NGC 5466 (Beccari et al. 2015), and 47 Tuc (Zhang et al. 2015). The general picture outlined in Webb et al. (2014a) is observed in M10, Pal4, Pal 14, NGC 5466 and 47 Tuc as all five clusters show clear signs of mass segregation (although to different degrees). For four of the clusters, the degree to which they are mass segregated is commensurate with their respective half-mass relaxation times t_{rh} and the effects of tidal stripping. Pal 14 on the other hand, despite a high present day t_{rh}, also shows clear evidence of mass segregation in its α profile (Frank et al. 2014). The authors therefore suggest that Pal 14 must have either been partially mass segregated at birth or was much more compact in the past. Curiously, the α profile in NGC 6101 is nearly constant suggesting that cluster has undergone no mass segregation. The observed differences between M10, Pal 4, Pal 14, NGC 6101, NGC 5466 and 47 Tuc suggest that additional studies on how the radial variation of the stellar mass function evolves with time, and its dependence on various cluster parameters, are required before the α profile of a cluster can be used to constrain its formation conditions and dynamical history.

In this study, we present the evolution of the radial variation in the stellar mass function for a large suite of N-body model clusters with different initial conditions. In Section 2 we discuss the full suite of simulations used in this study. In Section 3 we first explore how variations in α with clustercentric distance r ($\alpha(r)$) evolve as a function of time and fraction of mass lost for two specific model clusters in isolation. Then we identify the effects of an external tidal field, initial size, the IMF, primordial mass segregation, primordial binary fraction, initial cluster mass, orbit and black hole retention on the evolution of $\alpha(r)$. We also consider whether the mass range over which the slope of the stellar mass function is measured introduces any type of bias. Varying initial cluster mass, size, and orbit further allows us to explore how the evolution of $\alpha(r)$ depends on a cluster's tidal filling factor $\frac{r_m}{r_t}$. Each of our findings are discussed and summarized in Section 4, where we also identify three distinct stages in the evolution of $\alpha(r)$.

2 N-BODY MODELS

The 12 Gyr evolution of each model star cluster in our suite of simulations was simulated using the direct N-body code NBODY6 (Aarseth 2003). While some of the models used here have been presented in previous studies, we will summarize again the general parameters of the entire suite of simulations for clarity and provide additional details for any new models. The initial radial profile of each cluster is generated from a Plummer density profile (Plummer 1911) out to a cut-off radius of 10 times the initial half-mass radius $r_{m,i}$ of the cluster. While we consider model clusters with a range IMFs (see Table 1), in all cases the minimum and maximum initial stellar masses are equal to 0.1 and 50 $M_\odot$ respectively and stellar metalicities are set equal to 0.001. For clusters with a non-zero initial binary fraction, total binary masses are set equal to the sum of two stars drawn from the IMF and the masses of individual stars within the binary are randomly selected from a uniform distribution. The stellar evolution algorithms for single and binary stars are discussed in Hurley et al. (2000) and Hurley et al. (2002) and the initial distribution of binary periods and orbital eccentricities are taken from Duquennoy & Mayor (1991) and Heggie (1975) respectively. Clusters are modelled either in isolation or orbiting within a Milky Way-like potential made up of a $1.5 \times 10^{10} M_\odot$ point-mass bulge, a $5 \times 10^{10} M_\odot$ Miyamoto & Nagai (1975) disk (with $a = 4.5$ kpc and $b = 0.5$ kpc), and a logarithmic halo potential (Xue et al. 2008) that is scaled to ensure that the circular velocity at a galactocentric distance R_{gc} of 8.5 kpc is 220 km/s.

The first two model clusters for which we study the evolution of $\alpha(r)$ have initial masses of $3 \times 10^4 M_\odot$, $r_{m,i}$ of 1.1 pc and 6 pc and no primordial binaries. The initial distribution of stellar masses follows a Kroupa, Tout, & Gilmore (1993) IMF (K93), with

$$\frac{dN}{dm} = m^\alpha \tag{1}$$

and α equals -2.7 for $m > 1M_\odot$, -2.2 for $0.5 \leqslant m \leqslant 1M_\odot$, and -1.3 for $0.08 < m \leqslant 0.5M_\odot$. We initially model these two clusters in isolation (IRM1 and IMR6) to set a basis for comparing how different initial conditions alter the evolution of $\alpha(r)$. To study the effects of an external tidal field, we then model each cluster with a circular orbit at 6 kpc in the Milky Way-like potential. Due to the higher escape rates experienced by clusters in an external tidal field, all the subsequent model clusters have a larger initial number of particles and masses of $6 \times 10^4 M_\odot$ (unless otherwise specified). When orbiting at 6 kpc in the Milky Way-like potential, the $r_{m,i} = 1.1$ pc cluster (RM1) is considered to be our standard tidally under-filling cluster with $\frac{r_m}{r_t} = 0.04$, while the $r_{m,i} = 6$ pc cluster (RM6) is considered to be our standard tidally filling cluster with $\frac{r_m}{r_t} = 0.2$.

Table 1. Model Input Parameters

Name	Mass	$r_{m,i}$	R_p	e	S	$\frac{N_{B,i}}{N_{tot}}$	IMF
Isolated Clusters							
IRM1	$3\times10^4 M_\odot$	1.1 pc	n/a	n/a	0	0	K93
IRM6	$3\times10^4 M_\odot$	6 pc	n/a	n/a	0	0	K93
Clusters in External Tidal Fields							
Standard Tidally Filling and Under-filling Models							
RM1	$6\times10^4 M_\odot$	1.1 pc	6 kpc	0	0	0	K93
RM6 (IMFK93, NB0)	$6\times10^4 M_\odot$	6 pc	6 kpc	0	0	0	K93
Primordial Mass Segregation							
PMS0/IMFK01	$6\times10^4 M_\odot$	6 pc	6 kpc	0	0	0	K01
PMS10	$6\times10^4 M_\odot$	6 pc	6 kpc	0	0.1	0	K01
PMS25	$6\times10^4 M_\odot$	6 pc	6 kpc	0	0.25	0	K01
PMS50	$6\times10^4 M_\odot$	6 pc	6 kpc	0	0.5	0	K01
IMF							
IMF185	$6\times10^4 M_\odot$	6 pc	6 kpc	0	0	0	$\alpha_0 = 1.85$
IMF235	$6\times10^4 M_\odot$	6 pc	6 kpc	0	0	0	$\alpha_0 = 2.35$
IMFBPL	$6\times10^4 M_\odot$	6 pc	6 kpc	0	0	0	$\alpha_0 = -0.9$ for $0.1 < m < 0.5 M_\odot$ $\alpha_0 = -2.3$ for $0.5 \leqslant m \leqslant 50 M_\odot$.
Binary Fraction							
NB2	$6\times10^4 M_\odot$	6 pc	6 kpc	0	0	2%	K93
NB4 (BH0, E0R6RM6)	$6\times10^4 M_\odot$	6 pc	6 kpc	0	4%	0	K93
Mass [1]							
M30K	$3\times10^4 M_\odot$	6 pc	6 kpc	0	0	4%	K93
M60K	$6\times10^4 M_\odot$	6 pc	6 kpc	0	0	4%	K93
M80K	$8\times10^4 M_\odot$	6 pc	6 kpc	0	0	4%	K93
M110K	$1.1\times10^5 M_\odot$	6 pc	6 kpc	0	0	4%	K93
Size and Orbit [2]							
E0R6RM1	$6\times10^4 M_\odot$	1.1 pc	6 kpc	0	0	4%	K93
E05RP6RM1	$6\times10^4 M_\odot$	1.1 pc	6 kpc	0.5	0	4%	K93
E0R18RM1	$6\times10^4 M_\odot$	1.1 pc	18 kpc	0	0	4%	K93
E05RP6RM6	$6\times10^4 M_\odot$	6 pc	6 kpc	0.5	0	4%	K93
E0R18RM6	$6\times10^4 M_\odot$	6 pc	18 kpc	0	0	4%	K93
E09RP6RM6	$6\times10^4 M_\odot$	6 pc	6 kpc	0.9	0	4%	K93
E0R104RM6	$6\times10^4 M_\odot$	6 pc	104 kpc	0	0	4%	K93
Black Hole Retention							
BH25 ($\frac{N_{BH,retained}}{N_{BH,created}} = 0.25$)	$6\times10^4 M_\odot$	6 pc	6 kpc	0	0	4%	K93
BH50 ($\frac{N_{BH,retained}}{N_{BH,created}} = 0.5$)	$6\times10^4 M_\odot$	6 pc	6 kpc	0	0	4%	K93

[1] Webb et al. (2013), Leigh et al. (2013), Webb & Leigh (2015)
[2] Leigh et al. (2013), Webb & Leigh (2015)

To explore how other initial parameters may affect the evolution of $\alpha(r)$, we have run simulations of the standard tidally filling and under-filling cases but with a range of IMFs, initial degrees of mass segregation (S), initial binary fractions ($\frac{N_{B,i}}{N_{tot}}$), masses, orbits, and black hole retention fractions ($\frac{N_{BH,retained}}{N_{BH,created}}$). Table 1 contains a complete list of all the models used in this study. To generate model clusters with different IMFs, we have used the publicly available code McLuster (Küpper et al. 2011) to simulate clusters with power law IMFs ($\alpha_0 = 1.85$, $\alpha_0 = 2.35$), a Kroupa (2001) IMF (K01), and a broken power law (BPL) IMF ($\alpha_0 = -0.9$ for $0.1 < m < 0.5 M_\odot$ and $\alpha_0 = -2.3$ for $0.5 \leqslant m \leqslant 50 M_\odot$). McLuster was also used to generate primordially mass segregated clusters, which were assumed to have a Kroupa (2001) IMF so they could be compared to the aforementioned K01 model. McLuster imposes mass segregation following the method introduced

in Baumgardt, De Marchi & Kroupa (2008), which ensures that model clusters with different degrees of primordial mass segregation have the same density profile. Black hole retention is incorporated into our models by ensuring that the desired retention fraction of black holes are not given a velocity kick upon creation.

3 EVOLUTION OF THE RADIAL VARIATION IN THE STELLAR MASS FUNCTION

To measure the radial variation of the stellar mass function at each time step for each model, special care was taken to properly bin the data with respect to both clustercentric distance and mass. Maíz Apellániz & Úbeda (2005) found that a variable bin size, which ensures that the same number of stars in each mass bin, minimizes any numerical bias when determining a cluster's mass function. We also apply this approach to our division of the cluster into radial bins.

We initially calculate the global stellar mass function for all stars within 0.1 and 0.5 $M_{\odot}$. Stars are sub-divided into 6 different mass bins, with the bin sizes (dm) kept variable in order to have the same number of stars dN in each mass bin. The mean mass of all stars in a given mass bin is used to set the corresponding value of m. The slope of the global stellar mass function α_G is then set equal to the slope of a plot of $\log(\frac{dN}{dm})$ versus $\log(m)$. Next, we sub-divide all stars with masses between 0.1 and 0.5 $M_{\odot}$ into 10 radial bins such that each bin contains 10% of the sub-sample of stars. The mean clustercentric radius of all the stars in a given radial bin is used to set the corresponding value of r. α is then calculated within each radial bin, yielding $\alpha(r)$ at each time step.

3.1 Star Clusters in Isolation

Simulations of clusters in isolation yield the evolution of $\alpha(r)$ when stellar evolution and two-body relaxation are the only mechanisms driving cluster evolution. For our standard isolated clusters IRM1 and IRM6, we plot the value of $\alpha(r)$ between $0.1-0.5$ $M_{\odot}$ as a function of the natural logarithm of each radial bin at 0, 2, 4, 8 , and 12 Gyr in Figure 1. Each radial bin has been normalized by r_m to better compare clusters of different size.

Figure 1 illustrates the effect that mass segregation has on the slope of the mass function at different clustercentric distances. As massive stars migrate inwards and low-mass stars migrate outwards, $\alpha(r)$ will flatten in the inner regions and steepen (become more negative) in the outer regions of the cluster. Since $\alpha(r)$ is also affected by the radial variation of the local relaxation time, which increases with clustercentric distance, the inner $\alpha(r)$ profile will evolve more rapidly than the outer one. This second point is why the $\alpha(r)$ profile is not a linear function of clustercentric distance.

To quantify the evolution of radial variations in the stellar mass function, we calculate the slope, $\frac{d\alpha(r)}{d(ln(\frac{r}{r_m}))}$, of the line of best fit to $\alpha(r)$ versus $\ln(\frac{r}{r_m})$ at each time step; hereafter we refer to this slope simply as $\delta\alpha$. Figure 2 illustrates the evolution of $\delta\alpha$ as a function of both time (normalized by the cluster's instantaneous $t_{rh}(t)$) and α_G. The normalization of time by $t_{rh}(t)$, calculated using the formalism of Spitzer & Hart (1971), serves as a proxy for comparing clusters at similar dynamical ages as can be determined by observers.

As discussed in the Introduction, a number of studies have shown that α_G traces the fraction of stars lost by a cluster; hence comparing the evolution of $\delta\alpha$ to α_G allows us to establish a connection between two fundamental aspects of a cluster's dynamical evolution: internal mass segregation and stellar escape. In the specific case of our simulations of isolated clusters, escape is negligible and the only effect shown in this figure is that of internal mass segregation.

The left panel of Figure 2 shows the time evolution of $\delta\alpha$ and demonstrates how mass segregation expectedly leads to a progressive increase in the radial variation of α. Initially, as a cluster expands and undergoes mass segregation $\delta\alpha$ will decrease. The rate at which $\delta\alpha$ decreases initially scales with a cluster's t_{rh}, however differences in the structural evolution of the compact and extended clusters leads to the divergence of the two evolutionary tracks. In particular the smaller t_{rh} of the compact system implies that when it reaches the same value of $\frac{t}{t_{rh}(t)}$ as the extended system it has an earlier age and therefore a broader range of stellar masses; as a consequence of this, stars with masses between 0.1 and 0.5 $M_{\odot}$ are less segregated in the compact system than in the extended one. To illustrate this point we show in the left panel of Figure 1 the points corresponding to a few different ages on the tracks of the two systems.

Once core-collapse occurs, mass segregation stops while the relaxation time at all clustercentric distances is increasing, consistent with the findings of a number of previous studies showing that mass segregation either stops or significantly slows down in the post-core collapse phase (e.g. Giersz & Heggie 1996). During this second phase $\delta\alpha$ remains approximately constant since mass segregation has stopped, with the possibility of a mild increase due to the post-core collapse expansion. Since the extended cluster has not reached core collapse by the end of the simulation and $\delta\alpha$ is still decreasing, the different levels of mass segregation (as measured by $\delta\alpha$) reached by the two clusters after 12 Gyr is a consequence of their different dynamical histories and core-collapse times. The rate at which $\delta\alpha$ decreases for the extended cluster does however slow done, due the isolated cluster continuing to expand, so $\delta\alpha$ will not continue to decrease indefinitely. As shown in the right panel of Figure 2, even though these clusters are initially losing mass due to the stellar evolution of high-mass stars the global mass function for stars between 0.1 and 0.5 $M_{\odot}$ remains unaffected over 12 Gyr since they evolve in isolation and very few stars actually escape the cluster.

While the results of this section serve to illustrate the fundamental aspects of cluster internal dynamical evolution, clusters do not actually evolve in isolation and will lose stars over time. Hence we must turn to the more realistic case of globular clusters orbiting in a gravitational field in order to determine how $\delta\alpha$ evolves as a function of α_G when both relaxation and tidal stripping are affecting cluster evolution.

3.2 Star Clusters Evolving in an External Tidal Field

In order to explore how the presence of an external tidal field will alter the evolution of $\delta\alpha$, we take the $r_{m,i} = 1.1$ and 6 pc

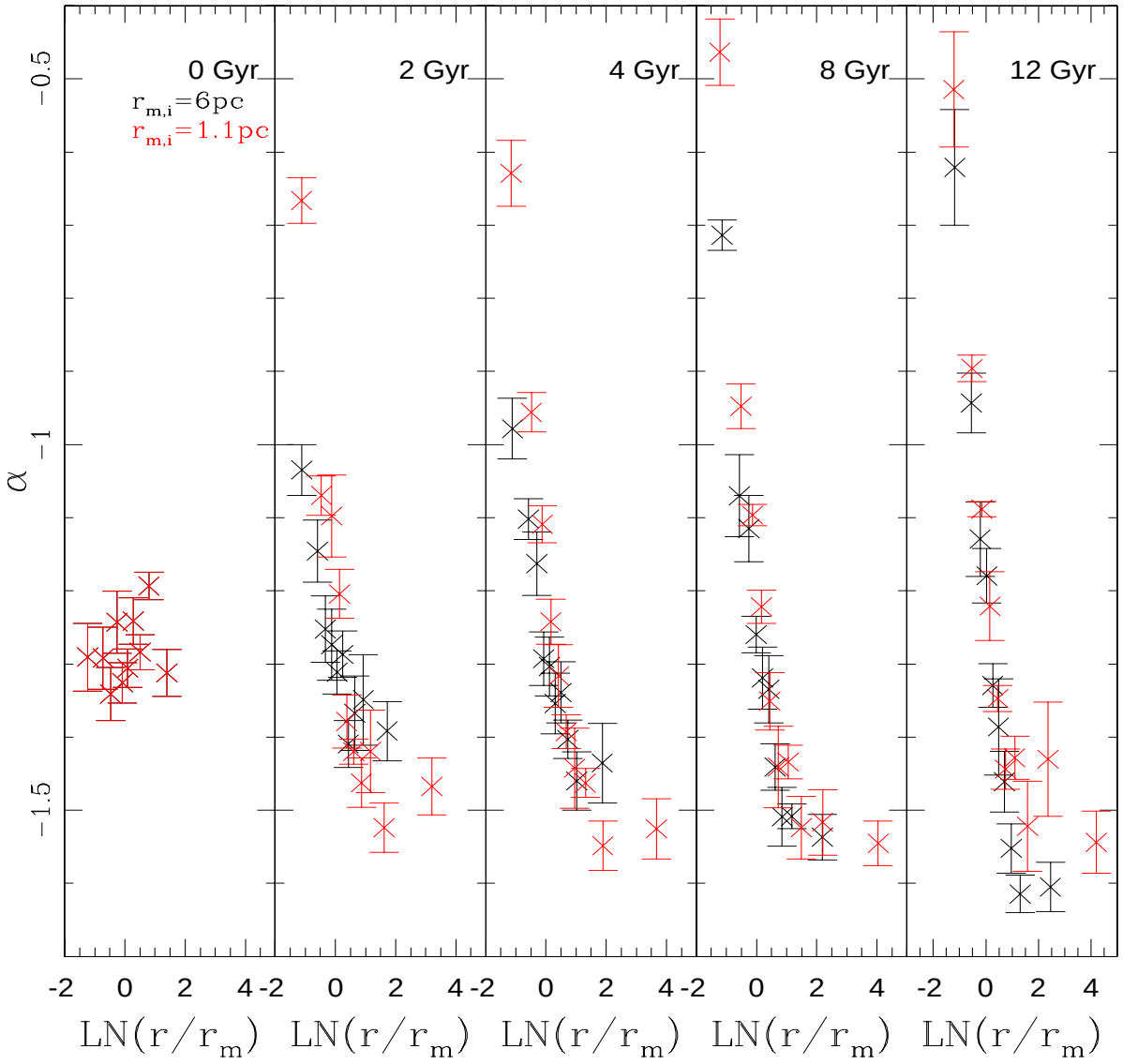

Figure 1. Slope of the stellar mass function for stars between 0.1- 0.5 $M_{\odot}$ at different clustercentric radii (normalized by r_m) for isolated globular clusters with initial masses of $3 \times 10^4 M_{\odot}$ and initial half mass radii of 1.1 pc (red) and 6 pc (black).

clusters that were previously evolved in isolation and study their evolution assuming they move on circular orbits at 6 kpc in a Milky Way-like tidal field. The evolution of $\delta\alpha$ with respect to both $\frac{t}{t_{rh}(t)}$ and α_G is illustrated in Figure 3.

An external tidal field has the primary effect of limiting the maximum size each cluster can reach and significantly enhance the rate of stellar escape compared to the isolated case. The resulting change to the evolution of $\delta\alpha$ is two-fold. Since each cluster will be smaller than if it were in isolation, the t_{rh} of each cluster is shorter and $\delta\alpha$ will decrease at a faster rate. Later, as $\delta\alpha$ decreases and the mean mass of escaping stars begins to decrease, the preferential escape of low-mass stars slows the decrease of α in the outer regions which in turn slows the decrease in $\delta\alpha$. The preferential escape of low-mass stars also causes a progressive flattening in the global mass function, as clearly illustrated by the evolution of $\delta\alpha$ with respect to α_G in the right panel Figure 3. Eventually the influence of low-mass stars being stripped from the cluster on $\delta\alpha$ becomes greater than the influence of low-mass stars segregating outwards, such that $\alpha(r)$ in the outer regions of the clusters starts to increase. Once $\alpha(r)$ begins increasing in the outer regions, $\delta\alpha$ will have reached its minimum value and will remain constant until the cluster reaches dissolution.

3.3 The Stellar Mass Function Over Different Mass Ranges and Timescales

We next consider whether the mass range over which the slope of the stellar mass function is measured will influence the evolution of $\delta\alpha$ as outlined in Sections 3.1 and 3.2. In Figures 4 and 5 we show the evolution of $\delta\alpha$ for the standard

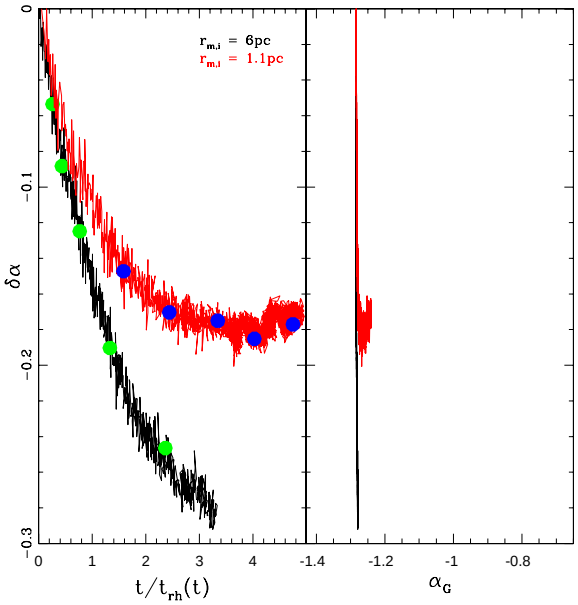

Figure 2. Slope of the radial variation in the stellar mass function for stars between 0.1- 0.5 $M_{\odot}$ as a function of time normalized by current relaxation time (left panel) and the global α_G (right panel) for isolated globular clusters with initial masses of $6.3 \times 10^4 M_{\odot}$ and initial half mass radii of 1.1 pc (red) and 6 pc (black). The blue and green filled circles mark 0.5 Gyr, 1 Gyr, 2 Gyr, 4 Gyr and 8 Gyr of evolution for the 1.1 pc and 6 pc model clusters respectively.

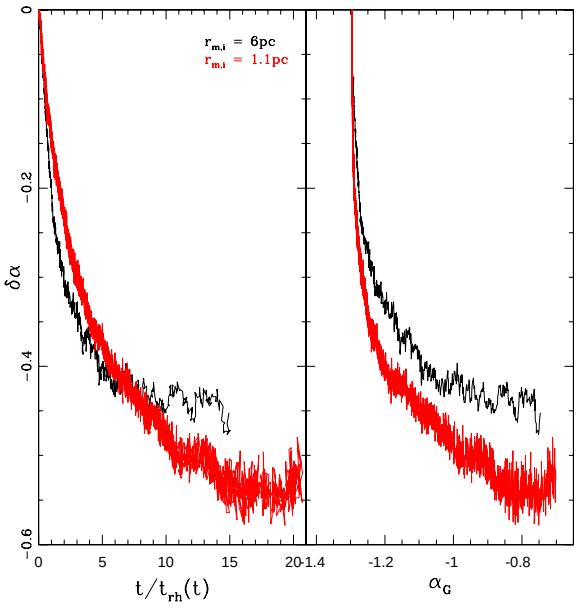

Figure 3. Slope of the radial variation in the stellar mass function for stars between 0.1- 0.5 $M_{\odot}$ as a function of time normalized by current relaxation time (left panel) and α_G (right panel) for globular clusters with circular orbits at 6 kpc, initial masses of $6.3 \times 10^4 M_{\odot}$, and initial half mass radii of 1.1 pc (red) and 6 pc (black).

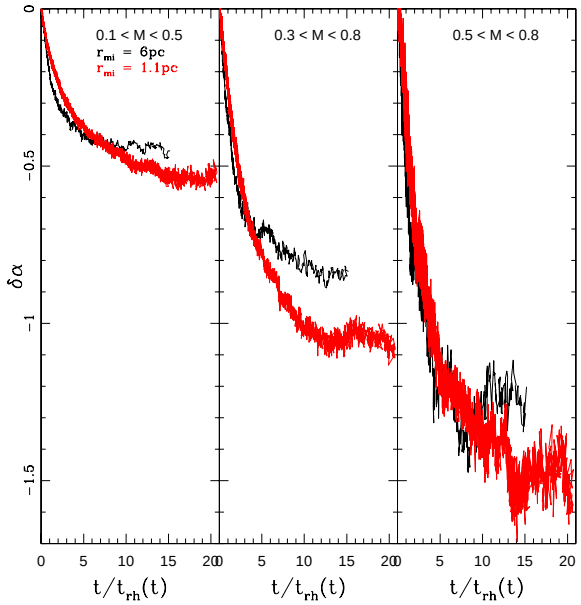

Figure 4. Slope of the radial variation in the stellar mass function for stars between 0.1 and 0.5 $M_{\odot}$ (left panel), 0.3 and 0.8 $M_{\odot}$ (center panel) and 0.5 and 0.8 $M_{\odot}$ (right panel) as a function of dynamical time for globular clusters with circular orbits at 6 kpc, initial masses of $6 \times 10^4 M_{\odot}$, and initial half mass radii of 1.1 pc (red) and 6 pc (black).

tidally filling and under-filling model clusters but with α measured over two other commonly used mass ranges: 0.3 - 0.8 $M_{\odot}$ and 0.5 - 0.8 $M_{\odot}$.

From Figures 4 and 5 we see that, as expected, stars in the higher mass ranges segregate more rapidly and reach a higher level of mass segregation than stars in lower mass ranges. Hence when measured using stars with $0.5 < m < 0.8 M_{\odot}$, $\delta\alpha$ is able to reach a lower minimum value before segregation slows compared to when stars between 0.1 and 0.5 $M_{\odot}$ are used. However, the evolution of $\delta\alpha$ is still qualitatively the same regardless of the mass range used to measure $\alpha(r)$.

3.4 The Initial Mass Function

In this section we study how the functional form of the IMF affects the evolution of $\alpha(r)$. We make this comparison in Figure 6, where we consider a Kroupa (2001) IMF, two power-law IMFs and a broken power-law IMF.

Figure 6 illustrates that dramatically changing the IMF of a cluster can alter the evolution of $\delta\alpha$. More specifically, if a different IMF results in a significant change to the cluster's t_{rh} or its structural evolution then the evolution of $\delta\alpha$ will change accordingly. Using the extreme case of a power-law IMF with $\alpha_{G,0} = -1.85$ as an example (IMF185), the large population of high-mass stars results in mass loss due to stellar evolution causing the cluster to undergo significant expansion at early times. A larger number of stars are therefore lost during the expansion process compared to the K93 case, with the cluster reaching a tidal filling factor greater than 0.325 when expansion due to stellar evolution is complete. Hence IMF185 will experience a higher stellar escape rate

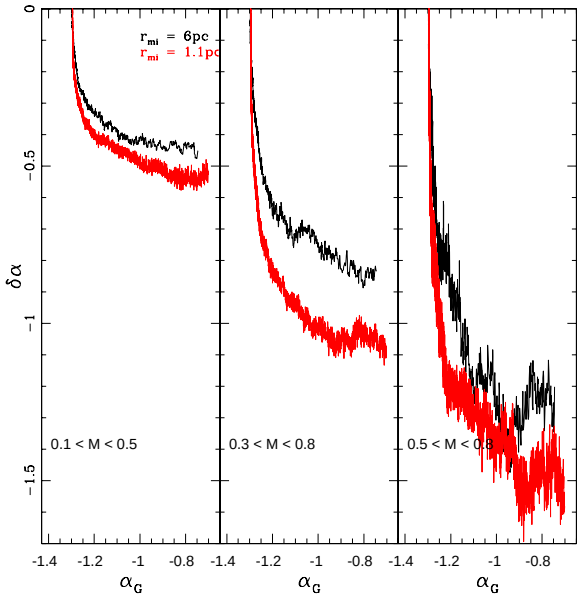

Figure 5. Slope of the radial variation in the stellar mass function for stars between 0.1 and 0.5 $M_\odot$ (left panel), 0.3 and 0.8 $M_\odot$ (center panel) and 0.5 and 0.8 $M_\odot$ (right panel) as a function of α_G for globular clusters with circular orbits at 6 kpc, initial masses of $6 \times 10^4 M_\odot$, and initial half mass radii of 1.1 pc (red) and 6 pc (black).

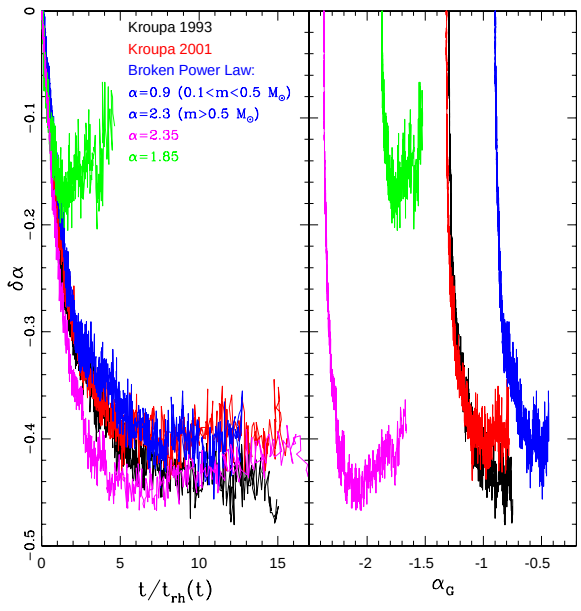

Figure 6. Slope of the radial variation in the stellar mass function for stars between 0.1- 0.5 $M_\odot$ as a function of time normalized by current relaxation time (left panel) and the global α_G (right panel) for globular clusters with circular orbits at 6 kpc, initial masses of $6.3 \times 10^4 M_\odot$, initial half mass radii 6 pc and different functional forms of their IMF.

than the more massive K93 model (Gieles, Heggie & Zhao 2011), and α_G will start evolving at a higher (less negative) value of δ_α. However it should be noted that a tidal filling factor greater than 0.325 is larger than all of the Galactic clusters except Pal 5 (Baumgardt et al. 2010).

For clusters that have IMFs that are more similar to IMFK93, such that there is not a major difference in their structural evolution, the evolution of $\delta\alpha$ with respect to $\frac{t}{t_{rh}(t)}$ appears to be independent of the functional form of the IMF. Model clusters IMFK01 ($\alpha_0 = -1.3$ for $0.1 < m < 0.5M_\odot$ and $\alpha_0 = -2.3$ for $0.5 \leqslant m \leqslant 50M_\odot$), IMF235 ($\alpha_{G,0} = -2.35$) and IMFBPL ($\alpha_0 = -0.9$ for $0.1 < m < 0.5M_\odot$ and $\alpha_0 = -2.3$ for $0.5 \leqslant m \leqslant 50M_\odot$) all segregate at similar rates as IMFK93. An observable difference between these model clusters can instead be found in the evolution of $\delta\alpha$ with respect to α_G. Clusters with different IMFs start with different initial values of α_G such that they are initially offset in the right panel of Figure 6. Since the relationship between $\delta\alpha$ and the amount that α_G changes from its initial value remains independent of the IMF, model clusters with bottom heavy (IMF235) or top heavy (IMFBPL) IMFs will never simultaneous reach the same $\delta\alpha$ and α_G as K93 or K01. Hence the $\delta\alpha$-α_G plane can be used to disentangle variations in the mass function slope due to a non-universal IMF from variations due to dynamical evolution and the preferential escape of low-mass stars.

3.5 Primordial Mass Segregation

A key assumption made in our previous models is that globular clusters are not primordially mass segregated and have an initial $\delta\alpha$ equal to 0. Not only will the initial $\delta\alpha$ of primordially mass segregated be non-zero, but they will undergo a larger initial expansion and therefore lose more stars via tidal stripping than a cluster with no primordial mass segregation (e.g. Baumgardt, De Marchi & Kroupa 2008; Vesperini et al. 2009; Haghi et al. 2015). To explore the effects of primordial mass segregation on the evolution $\delta\alpha$, we have modelled the evolution of our $r_{m,i} = 6$ cluster with a K01 IMF while adding varying degrees of primordial mass segregation (Figure 7).

Figure 7 illustrates that, as expected, a primordially mass segregated cluster will start its evolution with a more negative $\delta\alpha$ and is generally characterized by a more negative $\delta\alpha$ in the early phases of its evolution compared to a non-segregated cluster. Since primordially mass segregated clusters undergo a significant early expansion associated with mass loss due to stellar evolution (e.g. Baumgardt, De Marchi & Kroupa 2008; Vesperini et al. 2009; Haghi et al. 2015), $\delta\alpha$ will initially increase. When this expansion occurs, a large number of low-mass stars escape the cluster which also causes α_G to increase rapidly. It should be noted however that the global mass function over higher mass ranges ($0.3 < m < 0.8M_\odot$ or $0.5 < m < 0.8M_\odot$) will evolve more slowly since it is mainly low-mass stars that initially escape the clusters.

After the initial expansion phase, $\delta\alpha$ begins to decrease for the moderately segregated clusters (PMS10, PMS25) as each cluster resumes the mass segregation process. For the highly segregated cluster (PMS50), the early expansion re-

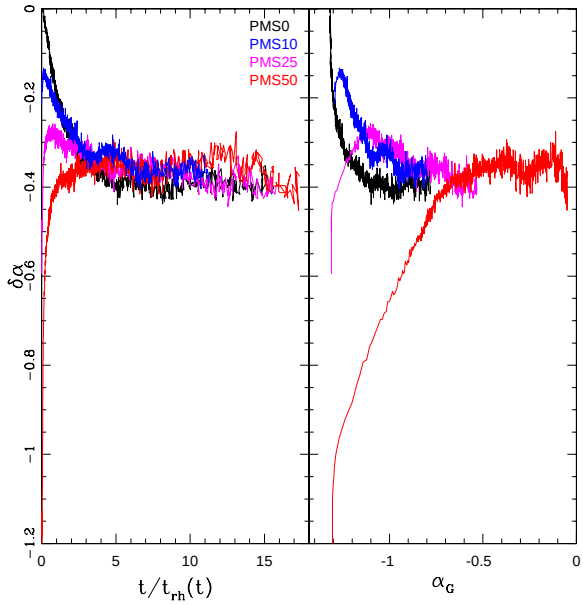

Figure 7. Slope of the radial variation in the stellar mass function for stars between 0.1 and 0.5 $M_{\odot}$ as a function of time normalized by current relaxation time (left panel) and the global α_G (right panel) for globular clusters with circular orbits at 6 kpc, initial masses of $6.3 \times 10^4 M_{\odot}$, initial half mass radii 6 pc and primordial segregation factors of 0 (black), 0.25 (magenta), 0.5 (red) and 0.9 (red).

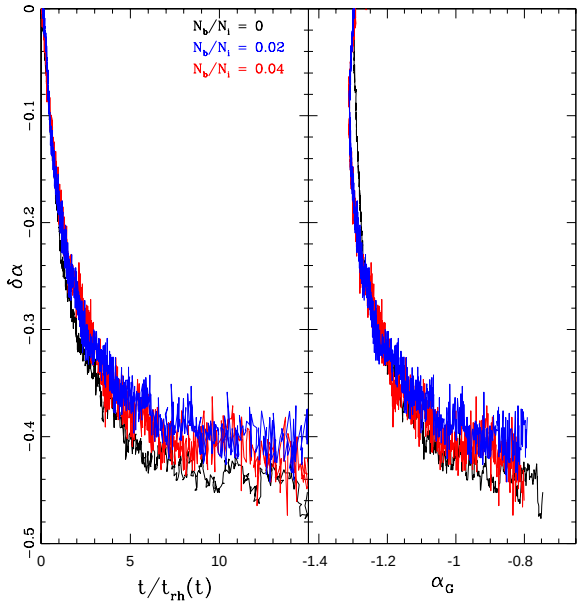

Figure 8. Slope of the radial variation in the stellar mass function for stars between 0.1- 0.5 $M_{\odot}$ as a function of time normalized by current relaxation time (left panel) and the global α_G (right panel) for globular clusters with circular orbits at 6 kpc, initial masses of $6.3 \times 10^4 M_{\odot}$, initial half mass radii 6 pc and initial binary fractions of 4% (black), 2% (blue) and 0% (red).

sults in a t_{rh} so long that the cluster is unable to segregate any further after its initial expansion.

The fact that each of these simulations converge to the same value of $\delta\alpha$ in the left panel of Figure 7 suggests that any effect primordial mass segregation has on the evolution of $\delta\alpha$ is lost after clusters begin losing stars via tidal stripping. However, the right panel of Figure 7 suggests the $\delta\alpha$-α_G plane could be used to identify clusters with stronger primordial mass segregation during the early stages of their evolution. Before $\delta\alpha$ reaches the asymptotic value of the unsegregated model, primordially mass segregated clusters will appear to have undergone significant mass segregation while maintaining a relatively unchanged mass function.

3.6 Initial Binary Fraction

Since globular clusters form with non-zero initial binary fractions, it is very important to determine whether the presence of primordial binaries can alter the evolution of $\delta\alpha$. To address this issue, we have modelled the evolution of the tidally filling cluster (NB0) with initial binary fractions of 2% (NB2) and 4% (NB4). Figure 8 shows that the time evolution of $\delta\alpha$ is not significantly affected by the presence of primordial binaries. Since binaries minimally affect neither the expansion rate or stellar escape rate of a cluster (and therefore do not affect its t_{rh}), $\delta\alpha$ for two clusters that have the same age can be directly compared without having to worry about whether or not the clusters had different binary fractions at birth.

Binaries do however influence the early measurement of α_G, as discussed in Webb & Leigh (2015). By treating binaries as unresolved, binary stars will initially appear as single high mass stars. As binary stars become unbound, an apparent influx of additional low-mass stars will occur causing α_G to initially decrease before increasing as the cluster loses mass. This is however a small effect and becomes negligible after clusters have lost 50% of their initial mass (see Webb & Leigh 2015).

3.7 Initial Cluster Mass

With an understanding that primordial binaries minimally affect the evolution of $\delta\alpha$, we can make use of previous simulations with initial binary fractions of 4% to study how initial cluster mass can influence the evolution of $\delta\alpha$. Initially presented in Webb et al. (2013), Leigh et al. (2013) and Webb & Leigh (2015), we have additional simulations of the tidally filling case with 4% binaries (M60K) but with initial masses between $3 \times 10^4 M_{\odot}$ and $1.1 \times 10^5 M_{\odot}$ (M30K, M80K, and M110K). The evolution of $\delta\alpha$ for each of these models is presented in Figure 9.

Since these models have the same $r_{m,i}$ and are evolved at a fixed galactocentric radius, models with different masses have different tidal filling factors, relaxation times, and star-escape/lifetime timescales. Differences in the evolution of δ_{α} versus $\frac{t}{t_{rh}(t)}$ (see the left panel of Figure 9) are therefore a consequence of the different rate of the structural and mass evolution for clusters with different initial masses. The higher mass clusters are more under-filling and lose mass at a slower rate than the low-mass clusters, such that they have more time to segregate before escaping stars cause $\alpha(r)$ to stop decreasing in the outer regions (in agreement with Section 3.2). Lower mass clusters on the other hand are more

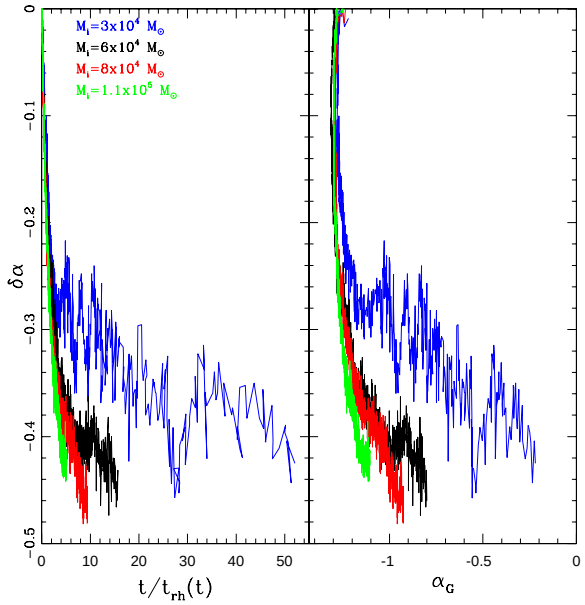

Figure 9. Slope of the radial variation in the stellar mass function for stars between 0.1- 0.5 $M_{\odot}$ as a function of time normalized by current relaxation time (left panel) and the global α_G (right panel) for globular clusters with circular orbits at 6 kpc, initial masses between $3\times10^4 M_{\odot}$ and $1.1\times10^5 M_{\odot}$, and initial half mass radii of 6 pc. Different model clusters are colour coded based on mass, as indicated by the legend.

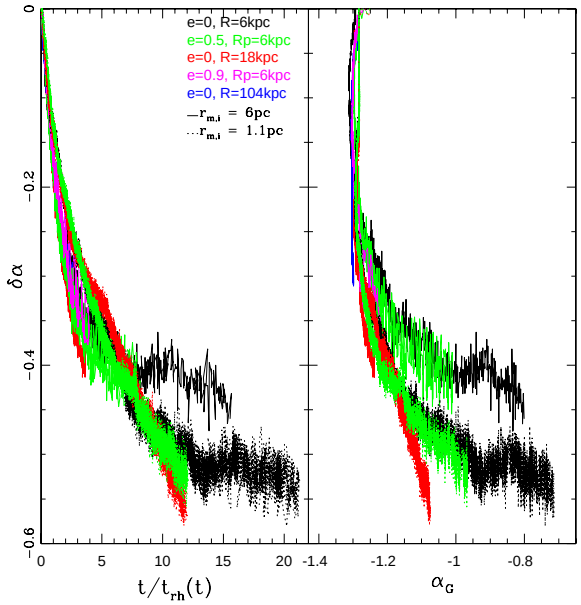

Figure 10. Slope of the radial variation in the stellar mass function for stars between 0.1- 0.5 $M_{\odot}$ as a function of time normalized by current relaxation time (left panel) and α_G (right panel) for globular clusters with circular orbits between 6 and 18 kpc, orbital eccentricities between 0 and 0.9, initial masses of $6\times10^4 M_{\odot}$, and initial half mass radii of 1.1 pc (dotted lines) and 6 pc (solid lines). Different model clusters are colour coded based on orbit, as indicated by the legend.

filling and characterized by smaller initial relaxation times, evolving towards even smaller values of $t_{rh}(t)$ after the initial expansion stage. Hence low-mass clusters reach a given value of $\frac{t}{t_{rh}(t)}$ earlier than higher mass clusters and are characterized by a smaller degree of mass segregation. Moreover, with the higher mass loss rate also experienced by lower mass clusters, $\alpha(r)$ stops decreasing in the outer regions of the cluster (causing the evolution of δ_α to slow down as well) at a lower $\frac{t}{t_{rh}(t)}$ compared to the high mass clusters. The relative widths of each clusters mass function do not play a significant role in the evolution of each δ_α here, as it did in Section 3.1, since the evolutionary track of the lowest mass cluster is identical to the other models for the first 4 Gyr.

Differences in relaxation times and different star-escape/lifetime timescales also dictate the extent of the model evolution of $\delta\alpha$ with respect to α_G. The more rapid rate of star escape in lower mass systems leads to a more rapid evolution towards flatter slopes for the mass function (see the right panel of Figure 9). Hence α_G in systems with lower masses is able to start evolving before significant mass segregation has occurred (as measured by $\delta\alpha$).

3.8 Initial Size and Cluster Orbit

To explore how a cluster's tidal filling factor affects $\delta\alpha$, we again make use of models from Leigh et al. (2013) and Webb & Leigh (2015) with initial binary fractions of 4% and $r_{m,i}$ = 1.1 pc and 6 pc. To compare with the standard tidal filling case (E0RP6RM6), we determine the evolution of $\delta\alpha$ for identical model clusters with circular orbits at 18 kpc (E0RP18RM6) and 104 kpc (E0RP104RM6) and with eccentric orbits that have perigalactic distances of 6 kpc and orbital eccentricities (e) of 0.5 ((E05RP6RM6) and 0.9 (E09RP6RM6). To compare with the standard tidally under-filling case (E0RP6RM1), we follow the evolution of $\delta\alpha$ for one model cluster with a circular orbit at 18 kpc (E0RP18RM1) and another with a perigalactic distance of 6 kpc and an orbital eccentricity of 0.5 (E05RP6RM1). The evolution of $\delta\alpha$ with respect to $t/t_{\rm rh}(t)$ and α_G for all 8 models is illustrated in Figure 10.

The interpretation of the evolutionary tracks shown in Figure 10 follows our discussion of models with different initial masses in Section 3.7. The evolution of $\delta\alpha$ and α_G is dictated by the internal relaxation time and the timescale of star loss. For example, two clusters on the same orbit (e.g. the model with $e = 0$ and $R = 6$ kpc) but different initial half-mass radii will lose stars at similar rates (dictated by the strength of the tidal field (see e.g. Gieles & Baumgardt (2008)), but the timescale of segregation will be shorter for the initially more compact cluster. As the two clusters lose stars and evolve towards smaller values of α_G, the more compact cluster will do so while converging to a smaller value of $\delta\alpha$ (i.e. a larger degree of mass segregation).

3.9 Black Hole Retention

Trenti et al. (2010) and Lutzgendorf et al. (2013) found that a population of dark remnants (black holes, neutron stars) or a massive black hole at the centre of the cluster will increase the escape rate of high-mass stars that have migrated to the centre of the cluster via mass segregation. Hence the

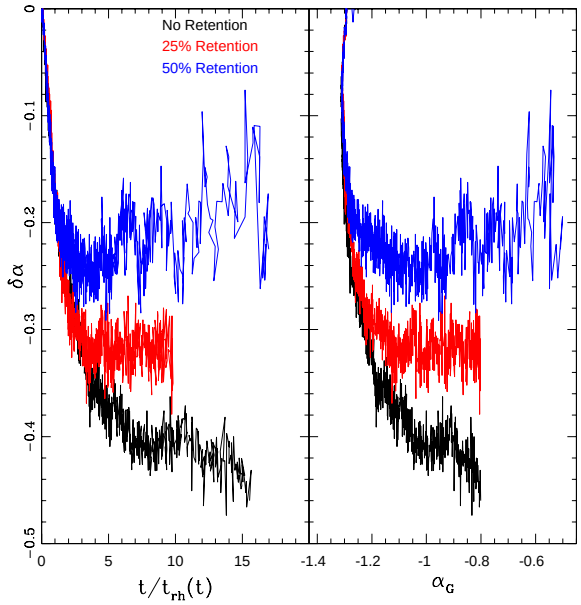

Figure 11. Slope of the radial variation in the stellar mass function for stars between 0.1- 0.5 $M_{\odot}$ as a function of time normalized by current relaxation time (left panel) and the global α_G (right panel) for globular clusters with circular orbits at 6 kpc, initial masses of $6.3 \times 10^4 M_{\odot}$, initial half mass radii 6 pc and dark remnant retention fractions of 0 (black), 0.25 (blue) and 0.5 (red).

global mass function will evolve at a slower rate as low-mass stars that have migrated outwards via mass segregation are not the only stars escaping the cluster. Furthermore, intermediate mass black holes have also been shown to quench mass segregation in globular clusters and may also influence the evolution $\delta\alpha$ (Gill et al. 2008; Pasquato et al. 2009). To determine whether the evolution of $\delta\alpha$ is affected by dark remnants, we have performed additional simulations with non-zero black hole retention fractions. More specifically we have re-simulated the tidally filling case with a circular orbit at 6 kpc and a binary fraction of 4% (BH0), but with 25% (BH25) and 50% (BH50) of newly created black holes not given velocity kicks at their time of formation such that they are retained by the cluster. The evolution of $\delta\alpha$ for all three models is illustrated in Figure 11.

From Figure 11 we see that black hole retention can slow and even completely halt the evolution of δ_{α}, in agreement with previous studies (Trenti et al. 2010; Lutzgendorf et al. 2013). The retention of black holes affects the mass segregation process in two different ways. First, a sub-population of near stellar mass black holes will migrate inwards and cause the core of the host star cluster to be much larger than if no black holes were retained. Hence the cluster's core relaxation time will increase and $\alpha(r)$ will increase in the inner regions of the cluster at a slower rate. δ_{α} will therefore be lower at a given $\frac{t}{t_{rh}(t)}$ for clusters with large black hole retention fractions.

Second, a sub-population of black holes will cause a cluster to initially expand to a larger r_m than if no black holes were retained such that the cluster becomes more tidally filling (Merritt et al. 2004; Mackey et al. 2008). Expanding to a larger filling factor means more stars escape the cluster during the expansion phase and $\alpha(r)$ will begin evolving from its primordial value at an earlier age, effectively halting the mass segregation process. Therefore, clusters with higher black hole retention fractions stop segregating at higher values of δ_{α} (less negative) than clusters that retain no black holes.

It should be noted that even if a cluster is able to retain a certain fraction of black holes when they first form, and have those black holes affect the evolution of its structural properties (and therefore δ_{α}), it does not mean the cluster contains each and every one of the retained black holes today. Dynamical evolution results in black holes continuously being ejected from the cluster's core. In fact, after 12 Gyr only 11% and 17% of all the black holes that were created remain in the model clusters with 25% and 50% retention fractions respectively. Hence a cluster will be more strongly affected by the retention of black holes than the present day black hole population would imply.

3.10 Projection Effects and Application to the Milky Way

In order to apply our models to observations of Galactic globular clusters, we must consider the evolution of δ_{α} when measured in projection. We first take the $r_{m,i} = 1.1$ and 6 pc model clusters on circular orbits at 6 kpc in a Milky Way-like tidal field (shown in Figure 3) and radially bin stars based on their projected clustercentric distance R. The line of best fit to $\alpha(R)$ versus $\ln(\frac{R}{R_m})$ at each time step is then calculated; hereafter we refer to this slope simply as $\delta_{\alpha,P}$. The evolution of $\delta_{\alpha,P}$ with respect to $\frac{t}{t_{rh}(t)}$ (which has been calculated using the cluster's projected half-mass radius) and the global mass function is plotted in Figure 12. It should be noted that to better compare with observations, we have used the more commonly observed mass range $0.3 < m < 0.8$ $M_{\odot}$ to illustrate the evolution of $\delta_{\alpha,P}$.

From Figure 12 we see that the general evolution of $\delta_{\alpha,P}$ is nearly identical to δ_{α} to within a scaling factor. The scaling factor is due to the fact that projection will lead to more low-mass stars *appearing* to be located in the inner regions of the cluster thus minimizing the inner $\alpha(R)$ profile. Hence $\delta_{\alpha,P}$ decreases less rapidly than its three-dimensional counterpart with respect to both $\frac{t}{t_{rh}(t)}$ and α_G.

In a future study we will carry out a dedicated investigation to compare the results of our simulations with observational data from a few wide field studies of Galactic globular clusters. We will further study all the aspects related to a direct comparison between observations and the results of numerical simulations. Factors such as the radial extent of observations, the range of masses observed, the completeness level of the observations can affect the values of $\delta_{\alpha,P}$ and their relation with the theoretical estimates of this quantity will all be considered.

4 DISCUSSION AND CONCLUSIONS

Motivated by recent observational studies that have been able to measure the radial variation in the stellar mass function of globular clusters, we have studied the time evolution of the radial variation of the stellar mass function's slope,

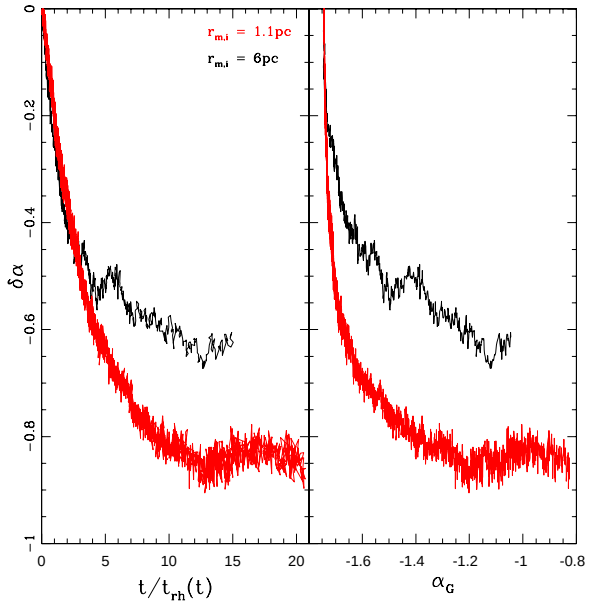

Figure 12. Slope of the projected radial variation in the stellar mass function for stars between 0.3- 0.8 $M_\odot$ as a function of time normalized by current relaxation time (left panel) and α_G (right panel) for globular clusters with circular orbits at 6 kpc, initial masses of $6.3 \times 10^4 M_\odot$, and initial half mass radii of 1.1 pc (red) and 6 pc (black).

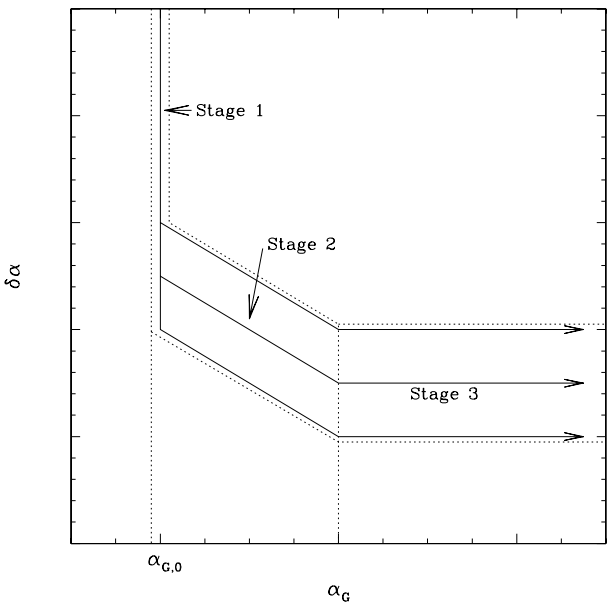

Figure 13. An schematic diagram illustrating the evolution of $\delta\alpha$ with respect to α_G for three clusters with different initial tidal filling factors. The evolution of $\delta\alpha$ has been broken down into three stages that are described in Section 4.

$\alpha(r)$, for a large suite of N-body star cluster simulations. In particular, we have focussed on how different initial sizes, masses, binary fractions, primordial mass segregation, black hole retention fractions, IMFs and external tidal fields affect the relationship between the time evolution of $\alpha(r)$ and the slope of the global mass function α_G measured over different mass ranges. We find that:

(i) In general the time evolution of $\alpha(r)$ is governed by the effects of internal two-body relaxation driving the system towards partial energy equipartition and mass segregation while the evolution with α_G is a consequence of the preferential escape of low-mass stars associated with two-body relaxation-driven mass loss. Our simulations show that the evolution of model clusters in the $\delta\alpha$-α_G plane can be separated into three distinct stages (see Figure 13):

- During the first stage, α_G does not evolve as the cluster is either not losing stars (because it is strongly underfilling) or is losing stars over the entire mass spectrum (because it is tidally filling but has not undergone mass segregation yet). $\delta\alpha$ will continually decrease as the effects of two-body relaxation lead to mass segregation and, as a result, $\alpha(r)$ in the inner and outer radial bins increasing and decreasing respectively. The rate at which $\delta\alpha$ decreases depends on the cluster's t_{rh} and its subsequent evolution; clusters with short relaxation times will segregate and evolve towards smaller values of $\delta\alpha$ more rapidly than clusters with long relaxation times.
- The second stage begins when the joint effects of mass segregation and stellar escape due to two-body relaxation become significant. As the cluster continues its evolution and starts to lose preferentially low-mass stars as a result of the effects of two-body relaxation, α_G begins to increase and the external tidal field begins affecting $\alpha(r)$ in the outer regions. During this stage, $\delta\alpha$ decreases at a slower rate because the rate at which low-mass stars segregate outward is balanced by the escape of preferentially low-mass stars from the cluster such that $\alpha(r)$ in the outermost regions stops decreasing.
- During the third and final stage, the preferential escape of low-mass stars from the cluster becomes dominant over the segregation of low-mass stars outwards and $\alpha(r)$ in the outer regions begins increasing such that $\delta\alpha$ remains constant in time and α_G continues to increase.

(ii) The minimum $\delta\alpha$ reached by a cluster is primarily dependent on its t_{rh} and how much it is able to segregate before stellar escapes causes $\alpha(r)$ in the outer regions to start increasing. The fact that all our model clusters reach similar minimum values of $\delta\alpha$ may be due to clusters not actually being able to evolve to a state of pure energy equipartition (Merritt 1981; Miocchi 2006; Trenti & van der Marel 2013; Gieles & Zocchi 2015; Bianchini et al. 2016), with the minimum $\delta\alpha$ representing the highest state of energy equipartition a star cluster can reach.

(iii) The position of a cluster on both the $\delta\alpha$-$t_{rh}(t)$ and $\delta\alpha$-α_G planes at a given age can provide a qualitative indication of its degree of primordial mass segregation and initial relaxation time relative to its present day properties or to other clusters. Clusters that have undergone significantly more segregation than their current $t_{rh}(t)$ or α_G would suggest likely had a shorter relaxation time in the past, were subject to a weaker tidal tidal field than their current orbit imposes, or were born primordially mass segregated.

(iv) Clusters that have different IMFs will be offset by their initial IMF slopes on the $\delta\alpha$-α_G plane such that the

degeneracy between variations in the slope of the present-day mass functions of globular clusters that are due to dynamical evolution and those due to a non-universal IMF can be lifted.

(v) Clusters with non-zero black hole retention fractions will undergo less segregation, and therefore have less negative values of δ_α, than clusters which retain no black holes due to the black hole sub-population causing the cluster's core radius and tidal filling factor to increase.

(vi) When measured in projection, clusters appear less segregated and therefore have less negative values of δ_α for a given $\frac{t}{t_{rh}(t)}$ and α_G. However, since the shape of the δ_α evolutionary tracks remain unchanged in projection, observations can still be used to constrain a cluster's IMF and draw qualitative conclusions regarding its degree of primordial mass segregation, initial relaxation time and initial tidal filling factor relative to its present day orbit and structure.

In light of the results shown by our theoretical study and the information that can be revealed by a full characterization of the radial variation of the slope of the PDMF, it is extremely important to further pursue wide field studies of Galactic globular clusters. In order to apply the results of our study to observations of globular clusters, special care must be taken to ensure models and observations are being compared over similar stellar mass ranges. However once these factors are taken into consideration, our study allows for the age, $\alpha(r)$, and α_G of a cluster to be used as a powerful tool for constraining the formation conditions and dynamical history of both globular clusters and their host galaxies.

ACKNOWLEDGEMENTS

This work was made possible in part by the facilities of the Shared Hierarchical Academic Research Computing Network (SHARCNET:www.sharcnet.ca) and Compute/Calcul Canada, in part by Lilly Endowment, Inc., through its support for the Indiana University Pervasive Technology Institute, and in part by the Indiana METACyt Initiative. The Indiana METACyt Initiative at IU is also supported in part by Lilly Endowment, Inc.

References

Aarseth, S.J. 2003, Gravitational N-body Simulations: Tools and Algorithms (Cambridge Monographs on Mathematical Physics). Cambridge University Press, Cambridge

Baumgardt H., Makino J. 2003, MNRAS, 340, 227

Baumgardt H., De Marchi G., Kroupa P. 2008, ApJ, 685, 247

Baumgardt, H., Parmentier, G., Gieles, M., Vesperini, E., 2010, MNRAS, 401, 1832

Beccari, G., Pasquato, M., De Marchi, G., Dalessandro, E., Trenti, M., Gill, M. 2010, ApJ, 713, 194

Beccari, G., Dalessandro, E., Lanzoni, B., Ferraro, F.R., Bellazzini, M., Sollima, A. 2015, ApJ, 814, 144

Bianchini, P., van de Ven, G., Norris, M. A., Schinnerer, E., Varri, A. L. 2016, MNRAS, Accepted, arXiv:1603.00878

Brockamp, M., Küpper, A. H. W, Ties, I., Baumgardt, H., Kroupa, P, 2014, MNRAS, 441, 150

Cai, M.X,, Gieles, M., Heggie, D.C., Varri, A.L. 2016, MNRAS, 455, 596

Dalessandro, E., Ferraro, F. R., Massari, D., Lanzoni, B., Miocchi, P., Beccari, G. 2015, ApJ, 810, 40

Duquennoy, A. & Mayor, M. 1991, A&A, 248, 485

Fall S. M., Zhang Q. 2001, ApJ, 561, 751

Frank, M.J., Hilker, M., Baumgardt, H., Ct, P., Grebel, E.K., Haghi, H., Kpper, A.H.W., Djorgovski, S. G. 2012, MNRAS, 423, 291

Frank, M.J., Grebel, E.K., Kpper, A.H. W. 2014, MNRAS, 443, 815

Gieles, M., Portegies Zwart, S.F., Baumgardt, H., Athanassoula, E., Lamers, H. J. G. L. M., Sipior, M., Leenaarts, J. 2006, MNRAS, 371, 793

Gieles, M. & Baumgardt, H. 2008, MNRAS, 389, L28

Gieles M., Heggie D., Zhao H. 2011, MNRAS, 413, 2509

Gieles, M. & Zocchi, A. 2015, MNRAS, 454, 576

Giersz M., Heggie D. C. 1996, MNRAS, 279, 1037

Gill, M., Trenti, M., Miller, M.C., van der Marel, R., Hamilton, D., Stiavelli, M. 2008, ApJ, 686, 303

Gnedin, O.Y., Lee, H. M., Ostriker, J. P., 1999, ApJ, 522, 935

Haghi, H., Zonoozi, A.H., Kroupa, P., Banerjee, S., Baumgardt, H. 2015, MNRAS, 454, 3872

Heggie, D.C. 1975, MNRAS, 173, 729

Heggie D. C., Hut P. 2003, The Gravitational Million-Body Problem: A Multidisciplinary Approach to Star Cluster Dynamics (Cambridge: Cambridge University Press)

Hurley, J. R., Pols, O.R., Tout, C.A. 2000, MNRAS, 315, 543

Hurley, J. R., Tout, C.A., Pols, O.R. 2002, MNRAS, 329, 897

Kroupa, P., Tout C.A., Gilmore, G. 1993, MNRAS, 262, 545

Kroupa P. 2001, MNRAS, 322, 231

Kruijssen, J.M.D. 2009, A&A, 507, 1409

Kruijssen, J.M.D., Pelupessy, F.I., Lamers, H.J.G.L.M., Portegies Zwart, S.F., Icke, V. 2011, MNRAS, 414, 2

Kruijssen, J.M.D., Pelupessy, F.I., Lamers, H.J.G.L.M., Portegies Zwart, S.F., Bastian, N., Icke, V. 2012, MNRAS, 421, 3

Küpper A. H. W., Maschberger, T., Kroupa, P., Baumgardt, H. 2011, MNRAS ,417, 2300

Lamers, H. J. G. L. M., Baumgardt, H., Gieles, M., 2013, MNRAS, 433, 1378

Leigh N., Umbreit S., Sills A., Knigge C., de Marchi G., Glebbeek E., Sarajedini A. 2012, MNRAS, 422, 1592

Leigh, N., Giersz, M., Webb, J.J., Hypki, A., de Marchi, G., Kroupa, P., Sills, A. 2013, MNRAS, 436, 3399

Lutzgendorf, N., Baumgardt, H., Kruijssen, J.M.D. 2013, A&A, 558, A117

Mackey, A. D., Wilkinson, M. I., Davies, M. B., Gilmore, G. F. 2008, MNRAS, 386, 65

Maíz Apellániz, J., Úbeda, L. 2005, ApJ, 629, 873

Marks M., Kroupa P., Baumgardt H. 2008, MNRAS, 386, 2047

Merritt, D, 1981, AJ, 86, 318

Merritt, D., Piatek, S., Portegies Zwart, S., Hemsendorf M. 2004, ApJ, 608 L25

Miocchi, P. 2006, MNRAS, 366, 227

Miyamoto, M. & Nagai, R. 1975, PASJ, 27, 533

Pasquato, M., Trenti, M., De Marchi, G., Gill, M., Hamil-

ton, D.P., Miller, M.C.; Stiavelli, M., van der Marel, R.P. 2009, ApJ, 699, 1511
Plummer, H.C. 1911, MNRAS, 71, 460
Renaud, F., & Gieles, M. 2013, MNRAS, 431L, 83
Rieder, S., Ishiyama, T., Langelaan, P., Makino, J., McMillan, S.L.W., Portegies Zwart, S. 2013, MNRAS, 436, 3695
Spitzer, L.J. & Hart, M.H. 1971, ApJ, 164, 399
Trenti M., van der Marel, R. 2013, MNRAS, 435, 3272
Trenti, M., Vesperini, E., Pasquato, M. 2010, ApJ, 708, 1598
Vesperini E., Heggie D. C. 1997, MNRAS, 289, 898
Vesperini, E., McMillan, S.L.W., Portegies Zwart, S. 2009, ApJ, 698, 615
Webb, J.J., Harris, W.E., Sills, A., Hurley, J.R. 2013, ApJ, 764, 124
Webb, J.J., Leigh, N., Sills, A., Harris, W.E., Hurley, J.R. 2014, MNRAS, 442, 1569
Webb, J.J., Sills, A., Harris, W.E., Hurley, J.R. 2014, MNRAS, 445, 1048
Webb, J.J. & Leigh, N. 2015, MNRAS, 453, 3278
Weinberg, M.D. 1994, AJ, 108,1414
Xue, X.X. et al., 2008, ApJ, 684, 1143
Zhang, C., Li, C., de Grijs, R., Bekki, K., Deng, L., Zaggia, S., Rubele, S., Piatti, A.E., Cioni, M.L., Emerson, J., For, B., Ripepi, V., Marconi, M., Ivanov, V.D., Chen, L. 2015, ApJ, 815, 95

This paper has been typeset from a TEX/ LATEX file prepared by the author.